


Role of Mcpip1 in obesity-induced hepatic steatosis as determined by myeloid and liver-specific conditional knockouts

Natalia Pydyn¹ , Dariusz Żurawek¹, Joanna Koziel², Edyta Kus³, Kamila Wojnar-Lason^{3,4}, Agnieszka Jaształ³, Mingui Fu⁵, Jolanta Jura¹ and Jerzy Kotlinowski¹

1 Department of General Biochemistry, Faculty of Biochemistry, Biophysics and Biotechnology, Jagiellonian University, Krakow, Poland

2 Department of Microbiology, Faculty of Biochemistry, Biophysics and Biotechnology, Jagiellonian University, Krakow, Poland

3 Jagiellonian Center for Experimental Therapeutics, Jagiellonian University, Krakow, Poland

4 Department of Pharmacology, Jagiellonian University Medical College, Krakow, Poland

5 Department of Biomedical Science and Shock/Trauma Research Center, School of Medicine, University of Missouri, Kansas City, MO, USA

Keywords

fatty liver; inflammation; MCP1; NAFLD; obesity

Correspondence

J. Kotlinowski, Department of General Biochemistry, Faculty of Biochemistry, Biophysics and Biotechnology, Jagiellonian University, Gronostajowa 7, Krakow 30-387, Poland

Tel: +48 12 66 46139

E-mail: j.kotlinowski@uj.edu.pl

(Received 23 October 2020, revised 25 March 2021, accepted 28 May 2021)

doi:10.1111/febs.16040

Monocyte chemoattractant protein-induced protein 1 (MCP1, *alias* Regnase 1) is a negative regulator of inflammation, acting through cleavage of transcripts coding for proinflammatory cytokines and by inhibition of NFκB activity. Moreover, it was demonstrated that MCP1 regulates lipid metabolism both in adipose tissue and in hepatocytes. In this study, we investigated the effects of tissue-specific Mcpip1 deletion on the regulation of hepatic metabolism and development of nonalcoholic fatty liver disease (NAFLD). We used control Mcpip1^{fl/fl} mice and animals with deletion of Mcpip1 in myeloid leukocytes (Mcpip1^{fl/fl}LysM^{Cre}) and in hepatocytes (Mcpip1^{fl/fl}Alb^{Cre}), which were fed chow or a high-fat diet (HFD) for 12 weeks. Mcpip1^{fl/fl}LysM^{Cre} mice fed a chow diet were characterized by a significantly reduced hepatic expression of genes regulating lipid and glucose metabolism, which subsequently resulted in low plasma glucose level and dyslipidemia. These animals also displayed systemic inflammation, demonstrated by increased concentrations of cytokines in the plasma and high *Tnfa*, *Il6*, *Il1b* mRNA levels in the liver and brown adipose tissue (BAT). Proinflammatory leukocyte infiltration into BAT, together with low expression of *Ucp1* and *Pparg1a*, resulted in hypothermia of 22-week-old Mcpip1^{fl/fl}LysM^{Cre} mice. On the other hand, there were no significant changes in phenotype in Mcpip1^{fl/fl}Alb^{Cre} mice. Although we detected a reduced hepatic expression of genes regulating glucose metabolism and β-oxidation in these mice, they remained asymptomatic. Upon feeding with a HFD, Mcpip1^{fl/fl}LysM^{Cre} mice did not develop obesity, glucose intolerance, nor hepatic steatosis, but were characterized by low plasma glucose level and dyslipidemia, along with proinflammatory phenotype. Mcpip1^{fl/fl}Alb^{Cre} animals, following a HFD, became hypercholesterolemic, but accumulated lipids in the liver at the same level as Mcpip1^{fl/fl} mice, and no changes in the level of soluble factors tested in the plasma were detected. We have demonstrated that Mcpip1 protein plays an important role in the liver homeostasis. Depletion of Mcpip1 in myeloid leukocytes, followed by

Abbreviations

ALT, alanine aminotransferase; AST, aspartate aminotransferase; BMI, body mass index; ECM, extracellular matrix; GTT, glucose tolerance test; HDL, high-density lipoprotein; HFD, high-fat diet; LDH, lactate dehydrogenase; LDL, low-density lipoprotein; NAFLD, nonalcoholic fatty liver disease; NASH, nonalcoholic steatohepatitis.

systemic inflammation, has a more pronounced effect on controlling liver metabolism and homeostasis than the depletion of *Mcpip1* in hepatocytes.

Introduction

Monocyte chemoattractant protein-induced protein 1 (MCP1P1, alias Regnase 1), encoded by the *ZC3H12A* gene, is a RNase that degrades mRNAs, pre-miRNAs, and viral RNAs [1]. MCP1P1 functions as a negative regulator of inflammation, by direct cleaving of transcripts coding for proinflammatory cytokines like IL-1 β , IL-6, IL-8, and IL-12 [2–5], and by indirect inhibition of NF κ B activity [6]. Apart from immunomodulatory effects, MCP1P1 activity was shown to regulate many biological processes, such as cell differentiation, angiogenesis, proliferation, and adipogenesis [7–9]. Adipogenesis of 3T3-L1 cells is inhibited via the degradation of C/EBP β and selected pre-miRNAs by MCP1P1 [9,10]. Additionally, the MCP1P1 level in human adipose tissue inversely correlates with patients' BMI [11]. Despite the results mentioned above, the functions of *Mcpip1* in liver metabolism and nonalcoholic fatty liver disease (NAFLD) progression remain obscure.

Previous studies have shown that *Mcpip1*-deficient mice spontaneously develop systemic inflammatory response, leading to splenomegaly, lymphadenopathy, hyperimmunoglobulinemia, and ultimately death within 12 weeks [3,12]. Similarly, a hematopoietic deficiency of *Mcpip1* resulted in severe systemic and multiorgan inflammation [13]. It was also shown that overexpression of *Mcpip1* reduces liver injury in septic mice, by inhibiting inflammatory reaction in macrophages [14]. Additionally, *Mcpip1* ameliorates liver damage, reduces inflammation, and promotes tissue regeneration in the hepatic ischemia/reperfusion injury model [15].

Nonalcoholic fatty liver disease describes a wide range of liver conditions affecting people who drink little to no alcohol. It is a chronic and progressive disease, characterized in the first stages by an excessive accumulation of triglycerides in hepatocytes [16]. Untreated NAFLD can progress from simple steatosis, to more severe nonalcoholic steatohepatitis (NASH), which is additionally characterized by liver inflammation and fibrosis [17]. Ultimately, NASH can further progress to cirrhosis and/or hepatocellular carcinoma, which over time might require liver transplantation [18].

In present study, we aimed to examine the contribution of *Mcpip1* to liver metabolism and the pathogenesis of NAFLD. Specifically, we used Cre-LoxP

technology to delete *Zc3h12a* gene encoding *Mcpip1* in myeloid leukocytes (*Mcpip1*^{fl/fl}LysM^{Cre}) and in hepatocytes (*Mcpip1*^{fl/fl}Alb^{Cre}). Myeloid cells are represented in the liver mostly by Kupffer cells that make up 80% of whole-body macrophages, which is the largest population of tissue macrophages in solid organs [19]. Crosstalk between Kupffer cells and hepatocytes, mediated for example by IL-1 β , was shown to promote hepatic triglyceride storage through IL-1 β -dependent suppression of PPAR α activity and subsequent inhibition of β -oxidation [20]. Also, blood monocytes infiltrating the liver during NAFLD are involved in its progression through the production of a vast array of proinflammatory mediators [21]. In our study, by comparing *Mcpip1*^{fl/fl}LysM^{Cre} and *Mcpip1*^{fl/fl}Alb^{Cre} animal models, we were able to analyze the tissue-specific effects of *Mcpip1* on liver metabolism and NAFLD development. Our results provide comprehensive data on the role of the *Mcpip1* expression in the myeloid leukocytes and hepatocytes in the regulation of metabolism and sterile inflammation.

Results

Deletion of *Mcpip1* in myeloid cells, but not in hepatocytes, results in dyslipidemia

Control *Mcpip1*^{fl/fl} animals used in this study were born in both *Mcpip1*^{fl/fl}LysM^{Cre} and *Mcpip1*^{fl/fl}Alb^{Cre} mice colonies. In the first analysis, we tested whether there is a difference between these animals. As compared in Fig. S1, there were no changes in mass, blood biochemistry, gene expression, nor in plasma cytokine concentrations in both *Mcpip1*^{fl/fl} control cohorts (Fig. S1). Thus, in the next figures, all data are presented with one control group. *Mcpip1*^{fl/fl}LysM^{Cre} animals were already characterized by Li and coworkers, who demonstrated diminished expression of *Zc3h12a* encoding *Mcpip1* in macrophages and spleens, but not in livers in comparison with *Mcpip1*^{fl/fl} littermates [22]. On the other hand, *Zc3h12a* expression was lower in the livers, but not in VAT of *Mcpip1*^{fl/fl}Alb^{Cre} mice (Fig. S2).

Starting from the 7th week of the experiment, *Mcpip1*^{fl/fl}LysM^{Cre} mice were characterized by reduced body weight, although they consumed an equal amount of food compared to *Mcpip1*^{fl/fl} mice (Fig. 1A,B,

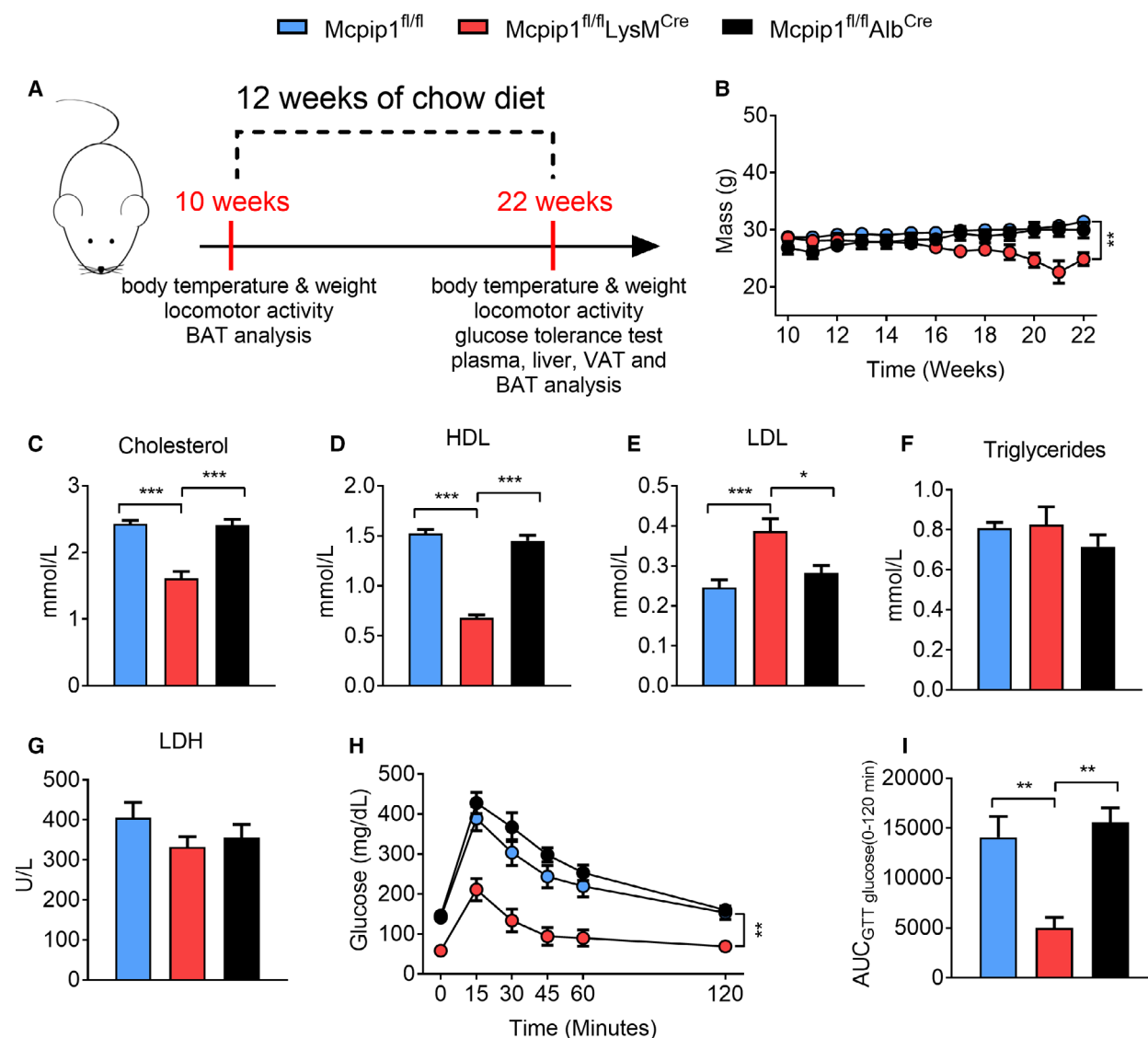


Fig. 1. Mcpip1^{fl/fl}LysM^{Cre} mice are characterized by reduced body weight, dyslipidemia, and low plasma glucose level. (A) Mcpip1^{fl/fl}, Mcpip1^{fl/fl}LysM^{Cre}, and Mcpip1^{fl/fl}Alb^{Cre} mice were analyzed at the age of 10 and 22 weeks. At 10 weeks of age, body temperature, weight, locomotor activity, and brown adipose tissue were analyzed. After feeding for 12 weeks with chow diet, we additionally performed glucose tolerance test, plasma, liver, and visceral adipose tissue analysis. (B) Body weight measurements of Mcpip1^{fl/fl}, Mcpip1^{fl/fl}LysM^{Cre}, and Mcpip1^{fl/fl}Alb^{Cre} mice fed chow diet. Plasma analysis of 22-week-old mice: (C) cholesterol; (D) HDL; (E) LDL; (F) triglycerides; (G) LDH levels. Glucose metabolism was tested after intraperitoneal injection of 2 g·kg⁻¹ of glucose, by (H) glucose tolerance test, and by (I) calculations of the area under the curve (AUC). For Mcpip1^{fl/fl}, *n* = 10 (B–G) and *n* = 8 (H, I); for Mcpip1^{fl/fl}LysM^{Cre}, *n* = 6 (B–G) and *n* = 5 (H, I); and for Mcpip1^{fl/fl}Alb^{Cre}, *n* = 8 (B–G) and *n* = 6 (H, I). The graphs show means ± SEM; **P* < 0.05; ***P* < 0.01; ****P* < 0.001.

Fig. S3A). At the age of 22 weeks, Mcpip1^{fl/fl}LysM^{Cre} exhibited hepatomegaly (0.053 ± 0.001 vs 0.037 ± 0.001 g), splenomegaly (0.029 ± 0.001 vs 0.004 ± 0.0004 g), and significantly lower cholesterol (1.6 ± 0.1 vs 2.4 ± 0.05 mmol·L⁻¹) and HDL (0.68 ± 0.02 vs 1.52 ± 0.03 mmol·L⁻¹) levels with concomitant increased concentration of LDL

(0.39 ± 0.03 vs 0.25 ± 0.01 mmol·L⁻¹), when compared to control Mcpip1^{fl/fl} mice (Fig. S3B,C, Fig. 1C–E). We did not observe differences in the concentration of triglycerides, nor activity of ALT, AST, and LDH in Mcpip1^{fl/fl}LysM^{Cre} animals compared with Mcpip1^{fl/fl} mice (Fig. 1F,G, Fig. S3D,E). Low plasma glucose level in Mcpip1^{fl/fl}LysM^{Cre} mice was demonstrated by

glucose tolerance test (Fig. 1H,I). Additionally, all measured analytes did not differ between control and *Mcpip1^{fl/fl}Alb^{Cre}* mice; however, *Mcpip1* depletion in hepatocytes resulted in hepatomegaly (0.037 ± 0.001 vs 0.046 ± 0.003 g) (Fig. 1C–I, Fig. S3B–E).

Mcpip1 depletion leads to liver pathology

Histological analysis of livers collected from *Mcpip1^{fl/fl}LysM^{Cre}* and *Mcpip1^{fl/fl}Alb^{Cre}* mice showed pathology of the bile ducts, each of them with different nature. Livers of *Mcpip1^{fl/fl}* mice did not show any pathological changes (Fig. 2A,B, left panel, proper bile ducts marked by asterisks, Fig. S4 left panel). The dominant pathology observed in *Mcpip1^{fl/fl}LysM^{Cre}* mice was located within large interstitial bile ducts and included hyperplasia and hypertrophy of cholangiocytes (Fig. 2A,B, middle panel, closed arrows, Fig. S4, middle panel). The hyalinization and ultimately cytoplasmic degranulation and cholangiocytes disintegration were also observed. Moreover, noted changes were accompanied by intense inflammatory infiltration (Fig. 2A, middle panel, open arrows, Fig. S4 middle panel) and local fibrosis (Fig. 2B, middle panel, arrowheads, Fig. S4, middle panel) without penetration into the liver parenchyma. Additionally, *Mcpip1^{fl/fl}LysM^{Cre}* mice were characterized by an increased extramedullary hematopoiesis in the liver located mainly in the walls of the sublobular veins, resulted in their significant thickening and fibrosis. The necrosis of single hepatocytes was found occasionally. In turn, histological analysis of livers collected from *Mcpip1^{fl/fl}Alb^{Cre}* mice revealed active and progressive proliferation of

intrahepatic bile ducts located peripherally (Fig. 2A, right panel, open arrows) accompanied by extensive parenchymal inflammation and fibrosis (Fig. 2B, right panel, arrowheads), along with fibrosis in portal areas (Fig. S4 right panel, asterisk) reflecting most of the features of human primary biliary cholangitis (PBC) (presented and discussed in details in [23]).

Myeloid and hepatic *Mcpip1* deletion alters expression of genes regulating glucose metabolism

In order to identify the molecular mechanism responsible for the low plasma glucose level and development of dyslipidemia in *Mcpip1^{fl/fl}LysM^{Cre}* animals, we analyzed a hepatic gene expression. The analysis revealed that *Mcpip1^{fl/fl}LysM^{Cre}* exhibits a significantly reduced expression of *G6pc* (regulating gluconeogenesis), *Irs1*, *Irs2* (response to insulin), and *Slc2a2* (glucose bidirectional transport) in livers (Fig. 3A). Changes in the livers of *Mcpip1^{fl/fl}Alb^{Cre}* mice were not as significant as in the case of *Mcpip1^{fl/fl}LysM^{Cre}*, we detected lower expression of *Pck1*, *G6pc*, and *Irs1* in comparison with *Mcpip1^{fl/fl}* mice (Fig. 3A).

Mcpip1 depletion disturbs lipid metabolism in the livers of *Mcpip1^{fl/fl}LysM^{Cre}* and *Mcpip1^{fl/fl}Alb^{Cre}* mice

Besides regulating glucose metabolism, the liver is also a prominent regulator of lipid metabolism, due to the ability to perform lipoprotein synthesis and lipid storage [24]. Therefore, in the following set of experiments,

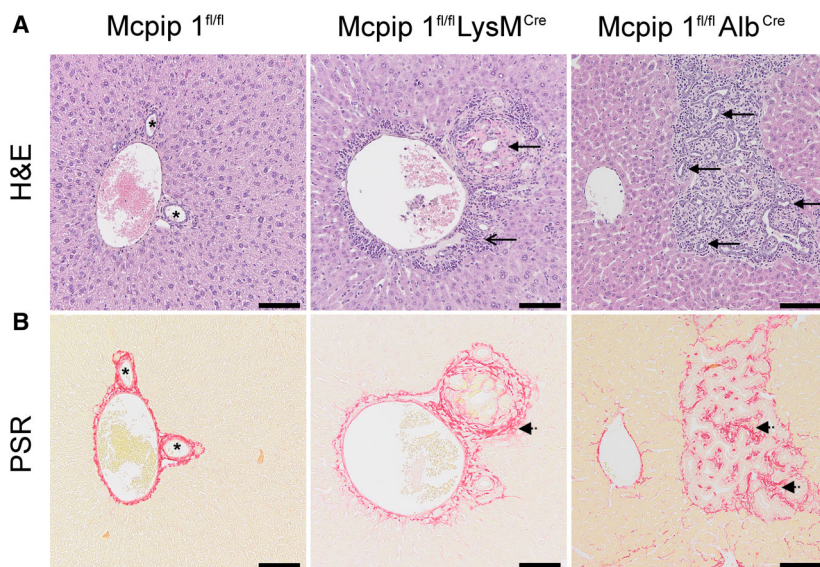


Fig. 2. *Mcpip1* depletion leads to liver pathology. Representative liver (A) hematoxylin and eosin (H&E) and (B) Picro Sirius Red (PSR) stainings. Asterisks point to proper bile ducts in control mice. Closed arrows point to dysplasia and proliferation of bile ducts with accompanying inflammation (open arrows) and collagen deposition (arrowheads) in *Mcpip1^{fl/fl}LysM^{Cre}* and *Mcpip1^{fl/fl}Alb^{Cre}* mice, respectively. The scale bar represents 200 μ m.

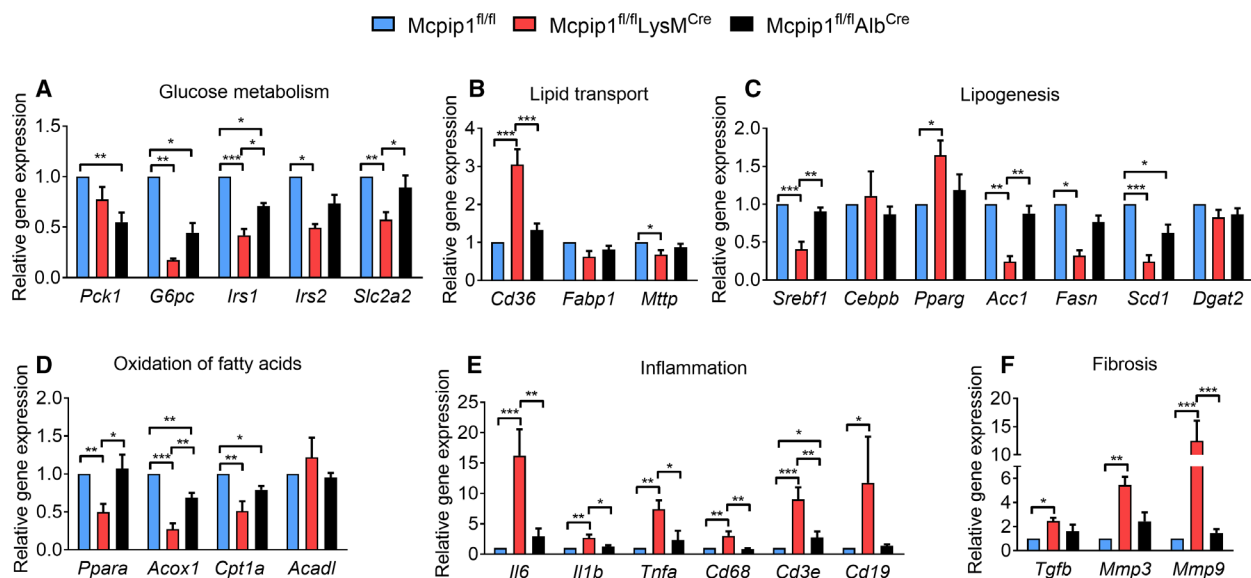


Fig. 3. Expression of *Mcpip1* is essential for proper liver metabolism. Expression of genes coding for proteins involved in (A) glucose metabolism; (B) lipid transport; (C) lipogenesis; (D) oxidation of fatty acids; (E) inflammation; and (F) fibrosis. For *Mcpip1*^{fl/fl}, *n* = 8; for *Mcpip1*^{fl/fl}LysM^{Cre}, *n* = 6; and for *Mcpip1*^{fl/fl}Alb^{Cre}, *n* = 9. The graphs show means ± SEM; **P* < 0.05; ***P* < 0.01; ****P* < 0.001.

we have evaluated the expression of key genes related to lipid transport, lipogenesis, and fatty acid oxidation. As shown in Fig. 3B–D, more significant changes in hepatic lipid metabolism were detected in *Mcpip1*^{fl/fl}LysM^{Cre} than in *Mcpip1*^{fl/fl}Alb^{Cre} mice (Fig. 3B–D). The expression of *Cd36* was increased, while *Mttp* was downregulated in the livers of *Mcpip1*^{fl/fl}LysM^{Cre} mice (Fig. 3B). Among the three master regulators of lipogenesis (*Srebf1*, *Cebpb*, *Pparg*) [25,26], we detected a lower expression of *Srebf1* in samples from *Mcpip1*^{fl/fl}LysM^{Cre} mice, together with the downregulation of SREBP1c-regulated genes, *Acc1*, *Fasn*, and *Scd1* (Fig. 3C). Furthermore, the expression of *Ppara* was reduced in the hepatic tissue of *Mcpip1*^{fl/fl}LysM^{Cre} mice, together with its downstream targets *Acox1* and *Cpt1a*, but not *Acadl* (Fig. 3D). In livers isolated from *Mcpip1*^{fl/fl}Alb^{Cre} animals, there were no differences in the expression of genes regulating lipid transport (*Cd36*, *Fabp1*, *Mttp*), but the amount of *Acox1*, *Cpt1a*, and *Scd1* transcripts was significantly reduced in comparison with control *Mcpip1*^{fl/fl} mice (Fig. 3B–D).

Deletion of *Mcpip1* in myeloid cells, but not in hepatocytes, induces systemic inflammation

To further characterize the phenotype of both *Mcpip1* knockout strains, we performed a Luminex Assay. Out of 45 analytes, 14 were not detected in all samples, whereas an expression of 20 was significantly changed between *Mcpip1*^{fl/fl}LysM^{Cre} and control mice

(Table 1). The level of cytokines and its receptors (*Tnf*-alpha, *Il-6* R alpha, *Tnf* RI, *Tnf* RII) was significantly upregulated in *Mcpip1*^{fl/fl}LysM^{Cre} in comparison with *Mcpip1*^{fl/fl} mice. Cytokines that are chemotactic for immune cells, for example, *Ccl8*, *Ccl12*, *Ccl19*, were significantly induced in *Mcpip1*^{fl/fl}LysM^{Cre} animals. Concentrations of other inflammation markers, such as *Syndecan-1/CD138*, *Chi3-L1*, and *p-Selectin*, were also increased in *Mcpip1*^{fl/fl}LysM^{Cre} animals compared with control mice (Table 1). In myeloid *Mcpip1* knockouts, we detected a reduced amount of three proteins, namely *Vegf-R2*, *thrombospondin 4*, and *endoglin*. Surprisingly, concentrations of all tested analytes were not changed between *Mcpip1*^{fl/fl} and *Mcpip1*^{fl/fl}Alb^{Cre} mice, indicating a key immunomodulatory role of myeloid *Mcpip1*.

Systemic inflammation in *Mcpip1*^{fl/fl}LysM^{Cre} mice was followed by a proinflammatory hepatic gene expression pattern. Expression of *Il6*, *Il1b*, as well as *Tnfa*, was significantly upregulated in the livers of *Mcpip1*^{fl/fl}LysM^{Cre} in comparison with *Mcpip1*^{fl/fl} mice. Livers of *Mcpip1*^{fl/fl}LysM^{Cre} were characterized by increased infiltration of macrophages, T and B lymphocytes, reflected by upregulated expression of *Cd68*, *Cd3e*, and *Cd19*. However, there were no changes between *Mcpip1*^{fl/fl} and *Mcpip1*^{fl/fl}Alb^{Cre} samples, beside increased expression of *Cd3e* (Fig. 3E). Moreover, we have found a significantly increased expression of profibrotic genes—*Tgfb*, *Mmp3*, and *Mmp9*—in the livers of *Mcpip1*^{fl/fl}LysM^{Cre}. On the other hand,

Table 1. Immune profile of plasma samples from 22-week-old mice determined by Luminex Assay. Out of 45 analytes, 14 has not been detected, namely IL-2, IL-1 β , IL-3, IL-7, CCL4/MIP-1 beta, CCL2/MCP1, RAGE, IL-17e/IL-25, IL-17/IL-17a, IL-1a, IL-4, IL-33, CCL5/RANTES, FGF-basic. For Mcpip1^{fl/fl} *n* = 6, for Mcpip1^{fl/fl}LysM^{Cre} *n* = 7, for Mcpip1^{fl/fl}Alb^{Cre} *n* = 7. The table shows means \pm SEM; nd, not detected.

Function	Analyte (pg·mL ⁻¹)	Mcpip1 ^{fl/fl}	Mcpip1 ^{fl/fl} LysM ^{Cre}	Mcpip1 ^{fl/fl} Alb ^{Cre}
Interleukins	IL-5	nd	0.047 \pm 0.013*	nd
	IL-6	nd	0.018 \pm 0.006*	nd
	IL-6 R alpha	14.99 \pm 1.06	30.12 \pm 2.41*	14.55 \pm 0.76
	IL-10	nd	0.030 \pm 0.007*	nd
	IL-12 p70	nd	0.140 \pm 0.065	nd
	IL-13	nd	0.252 \pm 0.025*	nd
	IL-16	0.463 \pm 0.104	0.561 \pm 0.174	0.434 \pm 0.075
	IL-27	nd	0.023 \pm 0.008*	nd
Chemokines	CCL8/MCP-2	127.16 \pm 10.59	525.62 \pm 60.80*	141.83 \pm 11.88
	CCL7/MARC	0.063 \pm 0.015	0.204 \pm 0.015*	0.060 \pm 0.019
	CCL12/MCP-5	0.027 \pm 0.011	0.280 \pm 0.037*	0.046 \pm 0.010
	CCL3/MIP-1 alpha	0.970 \pm 0.055	3.837 \pm 1.172*	0.890 \pm 0.051
	CCL20/MIP-3 alpha	0.126 \pm 0.040	0.097 \pm 0.048	0.028 \pm 0.028
	CCL19/MIP-3 beta	0.006 \pm 0.004	0.040 \pm 0.008*	0.0003 \pm 0.0002
	CCL11/Eotaxin	1.44 \pm 0.08	1.52 \pm 0.15	1.34 \pm 0.08
	CXCL16	0.358 \pm 0.027	0.203 \pm 0.045	0.267 \pm 0.053
Growth factors	GM-CSF	0.0005 \pm 0.0002	0.0009 \pm 0.0004	0.0004 \pm 0.0001
	M-CSF	4.84 \pm 1.03	2.55 \pm 0.48	6.73 \pm 1.68
	G-CSF	0.125 \pm 0.032	0.059 \pm 0.014	0.097 \pm 0.021
TNF	TNF-alpha	2.94 \pm 0.03	4.13 \pm 0.23*	2.97 \pm 0.09
	TNF RI	0.753 \pm 0.054	1.160 \pm 0.120*	0.759 \pm 0.046
	TNF RII	3.04 \pm 0.20	8.63 \pm 1.03*	3.48 \pm 0.49
Angiogenesis	VEGF	nd	0.0030 \pm 0.0006*	nd
	VEGF R2	49.70 \pm 2.11	29.77 \pm 2.13*	48.09 \pm 0.68
	Endoglin	1.88 \pm 0.30	1.00 \pm 0.14*	2.27 \pm 0.23
Others	Thrombospondin-4	705.99 \pm 99.09	380.89 \pm 46.32*	556.98 \pm 31.23
	CHI3-L1	29.40 \pm 3.70	145.56 \pm 21.41*	42.59 \pm 9.01
	Icam-1	18.06 \pm 2.37	13.69 \pm 2.36	17.88 \pm 0.75
	p-Selectin/CD-62P	29.01 \pm 4.49	46.23 \pm 8.13	29.09 \pm 4.93
	Syndecan-1/CD138	4.58 \pm 0.74	17.51 \pm 5.14*	7.13 \pm 0.69
	IFN gamma	0.03100 \pm 0.00007	0.0320 \pm 0.0002	0.03100 \pm 0.00009

P* < 0.05; *P* < 0.01; ****P* < 0.001.

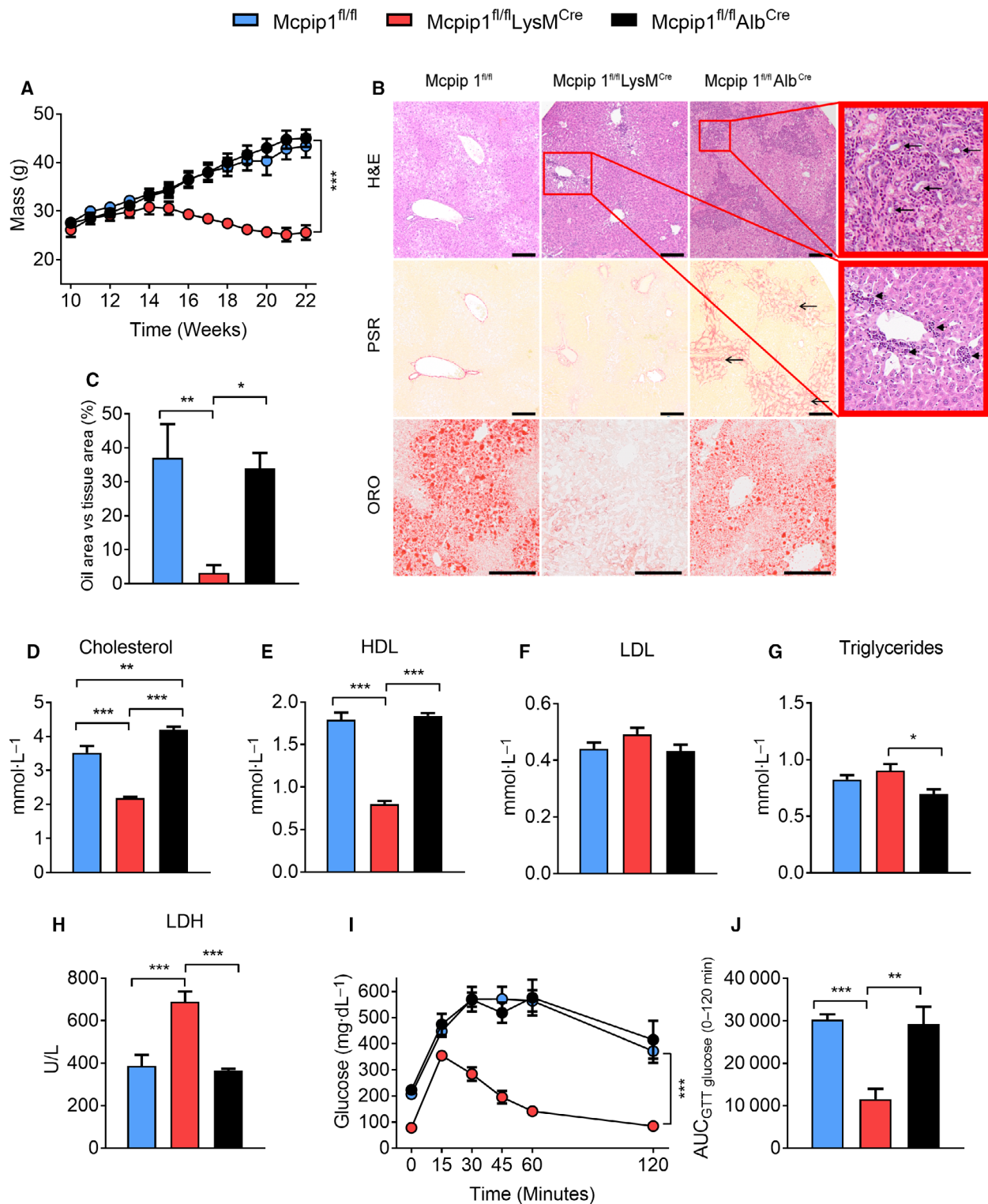
Mcpip1^{fl/fl}Alb^{Cre} mice were characterized by slightly, but not significantly higher expression of these selected genes (Fig. 3F).

High-fat diet does not induce obesity and hepatic steatosis in Mcpip1^{fl/fl}LysM^{Cre} mice

In agreement with literature data, High-fat diet (HFD) feeding increased body mass and liver steatosis of

Mcpip1^{fl/fl} mice (Fig. 4A–C). However, starting from the sixth week of experiment, Mcpip1^{fl/fl}LysM^{Cre} mice were characterized by significantly decreased body weight that cannot be fully attributed to lower food consumption (Fig. 4A, Fig. S5A). Additionally, Mcpip1^{fl/fl}LysM^{Cre} mice, after 12 weeks of HFD, were characterized by very limited liver steatosis (3% vs 37% in Mcpip1^{fl/fl}) (Fig. 4B and Fig. S6 middle panel, Fig. 4C), hepatomegaly (0.059 \pm 0.002 vs 0.031 \pm 0.001 g),

Fig. 4. Mcpip1^{fl/fl}LysM^{Cre} mice do not develop obesity and hepatic steatosis upon feeding with high-fat diet. Body weight measurements of Mcpip1^{fl/fl}, Mcpip1^{fl/fl}LysM^{Cre}, and Mcpip1^{fl/fl}Alb^{Cre} mice fed high-fat diet for 12 weeks. (B) Representative liver hematoxylin & eosin (H&E), Picro Sirius Red (PSR), and Oil Red O (ORO) stainings; arrowheads point to hematopoietic foci in Mcpip1^{fl/fl}LysM^{Cre}. Close arrows point to proliferation of intrahepatic bile ducts accompanying by pronounced inflammation and collagen deposition (open arrows) in Mcpip1^{fl/fl}Alb^{Cre} mice. The scale bar represents 200 μ m. (C) Quantitative analysis of Oil Red O-stained liver tissues; plasma analysis of 22-week-old mice: (D) cholesterol; (E) HDL; (F) LDL; (G) triglycerides; (H) LDH levels. Glucose metabolism was tested after intraperitoneal injection of 2 g·kg⁻¹ of glucose by (I) glucose tolerance test and by (J) calculations of the AUC. For Mcpip1^{fl/fl}, *n* = 7; for Mcpip1^{fl/fl}LysM^{Cre}, *n* = 6; and for Mcpip1^{fl/fl}Alb^{Cre}, *n* = 6. The graphs show means \pm SEM; **P* < 0.05; ***P* < 0.01; ****P* < 0.001.



splenomegaly (0.031 ± 0.003 vs 0.002 ± 0.0003 g), (Fig. S5B,C), and diffuse hematopoietic foci (Fig. 4B, middle panel, arrowheads). On the other hand, 12 weeks

of HFD feeding to Mecip1^{fl/fl}Alb^{Cre} mice resulted in hepatomegaly (0.045 ± 0.001 vs 0.031 ± 0.001 g), (Fig. S5B) without impact on body mass nor liver

steatosis (Fig. 4A,B). No changes in Mcpip1^{fl/fl}Alb^{Cre} mice phenotype, characterized as in chow diet fed mice by very pronounced collagen deposition (Fig. 4B, right panel, open arrows) and inflammation (Fig. 4B, right panel, orange closed arrows) accompanying proliferation of intrahepatic bile ducts (Fig. 4B, right panel, black closed arrows), were observed after HFD as well. Changes in lipid profile measured in plasma of both Mcpip1 knockouts, after 12 weeks of HFD, resembled results obtained in mice fed chow food: We detected low cholesterol (2.19 ± 0.03 vs 3.53 ± 0.19 mmol·L⁻¹) and HDL (0.80 ± 0.04 vs 1.79 ± 0.08 mmol·L⁻¹) concentration only in Mcpip1^{fl/fl}LysM^{Cre} mice (Fig. 4D,E). Twelve weeks of HFD increased the LDL level in Mcpip1^{fl/fl} in comparison with chow diet (0.44 ± 0.02 vs 0.25 ± 0.01 mmol·L⁻¹), blunting differences between these mice and myeloid knockouts (Fig. 4F). There were no changes in the LDL, triglycerides, ALT, and AST in Mcpip1^{fl/fl}LysM^{Cre} when compared to Mcpip1^{fl/fl} mice (Fig. 4F,G, Fig. S5D,E). Only the LDH level was raised in the plasma of Mcpip1^{fl/fl}LysM^{Cre} mice (689.00 ± 48.42 vs 387.57 ± 52.26 U·L⁻¹) (Fig. 4H). Mcpip1^{fl/fl}Alb^{Cre} mice were characterized by increased cholesterol level (4.20 ± 0.08 vs 3.53 ± 0.19 mmol·L⁻¹), but all other analytes did not differ between these animals and Mcpip1^{fl/fl} (Fig. 4D–H, Fig. S5D,E). Finally, feeding with HFD led to hyperglycemia and an impaired glucose tolerance detected in all three strains in comparison with mice fed a chow diet (Fig. 4I,J). However, based on GTT test and fasting glucose measurement, Mcpip1^{fl/fl}LysM^{Cre} animals were characterized by low plasma glucose level, in comparison with Mcpip1^{fl/fl} counterparts (Fig. 4I,J).

The profile of cytokines, chemokines, and growth factors in the plasma of HFD-fed mice showed similar tendencies to animals fed chow food (Table S3). Concentrations of proinflammatory mediators (interleukins, chemokines, soluble receptors, and ECM proteins) were significantly increased in Mcpip1^{fl/fl}LysM^{Cre} mice compared with their Mcpip1^{fl/fl} counterparts (Table S3). Again, there were no differences between Mcpip1^{fl/fl}Alb^{Cre} and Mcpip1^{fl/fl} mice. Interestingly, HFD feeding of Mcpip1^{fl/fl}LysM^{Cre} mice further elevated the amount of MIP-1 alpha, syndecan-1, and CHI3-L1, in comparison with animals on chow food (Table 1, Table S3).

Mcpi1 deficiency changes hepatic mRNA expression profile in HFD-fed mice

The expression of key gluconeogenesis regulators (*Pck1*, *G6pc*) was not changed in myeloid knockouts,

but impaired glucose metabolism in these mice is at least partially explained by a low level of *Irs1* and *Slc2a2* (Fig. 5A). Lipid metabolism was also altered in Mcpip1^{fl/fl}LysM^{Cre} animals fed for 12 weeks with HFD, as manifested by the reduced expression of *Fabp1* and *Mttp* regulating lipid transport, and low levels of *Srebfl1*, *Acc1*, *Fasn*, and *Scd1* mRNAs that are involved in lipogenesis (Fig. 5B,C). Additionally, the expression of genes regulating beta-oxidation (*Ppara*, *Acox1*, and *Cpt1a*) was significantly reduced in Mcpip1^{fl/fl}LysM^{Cre} mice (Fig. 5D). Additionally, there was a significant increase of proinflammatory and profibrotic transcripts in Mcpip1^{fl/fl}LysM^{Cre} mice in comparison with their Mcpip1^{fl/fl} counterparts (Fig. 5E,F).

High-fat diet feeding for 12-week blunted differences between Mcpip1^{fl/fl}Alb^{Cre} and Mcpip1^{fl/fl} mice. Out of 26 tested genes, only the level of *Pck1* was decreased in comparison with controls (Fig. 5A–F). Overall changes in the hepatic gene expression pattern in HFD-fed mice—Mcpip1^{fl/fl}LysM^{Cre} and Mcpip1^{fl/fl}Alb^{Cre} knockouts vs Mcpip1^{fl/fl}—were very similar to mice fed chow food (Figs 3A–F and 5A–F). Thus, our results indicate that the deletion of Mcpip1 protein in myeloid leukocytes has a more severe impact on metabolic regulatory function than hepatic Mcpip1 deficiency. Additionally, Mcpip1 acts independently from HFD-induced obesity effects on liver metabolic regulation.

Myeloid Mcpi1 deficiency changes production of adipokines by white adipose tissue

In order to analyze the lean phenotype of Mcpip1^{fl/fl}LysM^{Cre} mice (Fig. 6A), we evaluated visceral white adipose tissue deposits and performed indirect calorimetry measurements at 10- and 22-week time points. Body mass was unchanged (Fig. S7A) and visceral fat (VAT) was characterized by slightly decreased total mass in 10-week-old Mcpip1^{fl/fl}LysM^{Cre} animals in comparison with controls (Fig. S7B). In 22-week-old Mcpip1^{fl/fl}LysM^{Cre} mice, VAT mass was significantly reduced (0.001 ± 0.0003 vs 0.010 ± 0.001 g) with concomitant altered gene expression profile (Fig. 6B–F). Out of four tested adipokines (leptin, resistin, adiponectin, fatty acid-binding protein 4), the expression of *Lep* was downregulated by 83.1%, while *Retn* was increased by 130% in VAT of Mcpip1^{fl/fl}LysM^{Cre} mice (Fig. 6C). Transcripts of genes involved in glucose metabolism (*Insr*, *Slc2a4*) were not changed, but the mRNA level of *Cpt1a* was significantly reduced, and *Pnpla2* (encoding adipose triglyceride lipase) was enhanced in VAT collected from Mcpip1^{fl/fl}LysM^{Cre} animals (Fig. 6D,E). The mRNA levels of proinflammatory cytokines (*Il6*, *Il1b*, *Tnfa*),

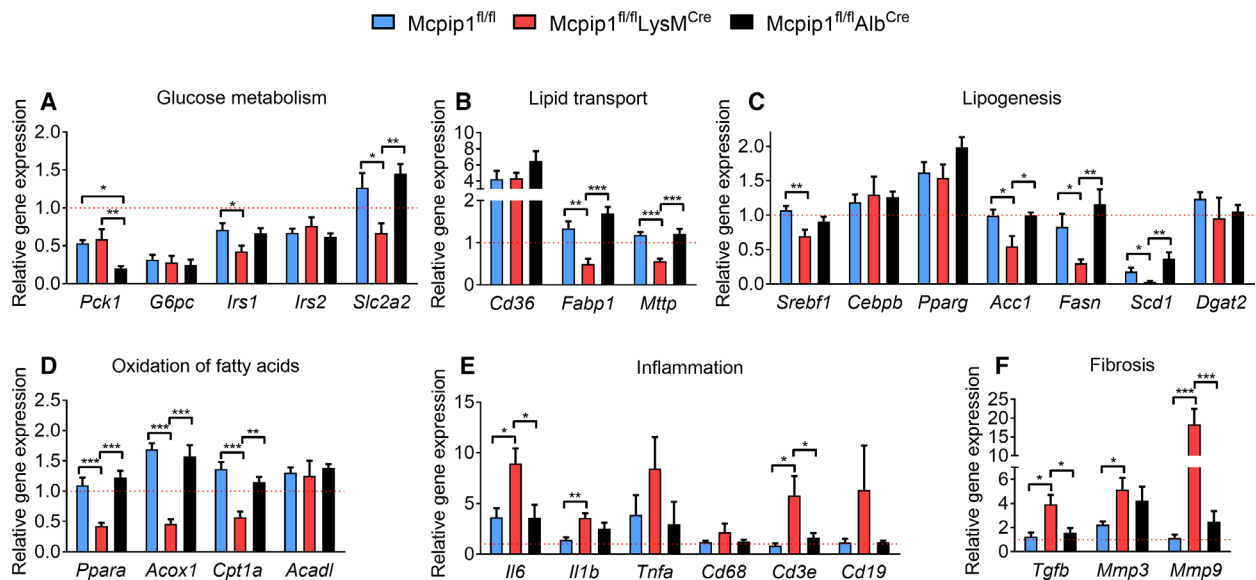


Fig. 5. Disturbed hepatic gene expression profile is linked to lean phenotype of HFD-fed *Mcpip1^{fl/fl}LysM^{Cre}* mice. Expression of genes coding for proteins involved in (A) glucose metabolism; (B) lipid transport; (C) lipogenesis; (D) oxidation of fatty acids; (E) inflammation; and (F) fibrosis. All results were calculated in comparison with appropriate gene in *Mcpip1^{fl/fl}* mice fed chow diet ($\Delta\Delta Ct$ method). Dotted lines represent results obtained from *Mcpip1^{fl/fl}* mice fed chow diet. For *Mcpip1^{fl/fl}*, $n = 7$; for *Mcpip1^{fl/fl}LysM^{Cre}*, $n = 8$; and for *Mcpip1^{fl/fl}Alb^{Cre}*, $n = 9$. The graphs show means \pm SEM; * $P < 0.05$; ** $P < 0.01$; *** $P < 0.001$.

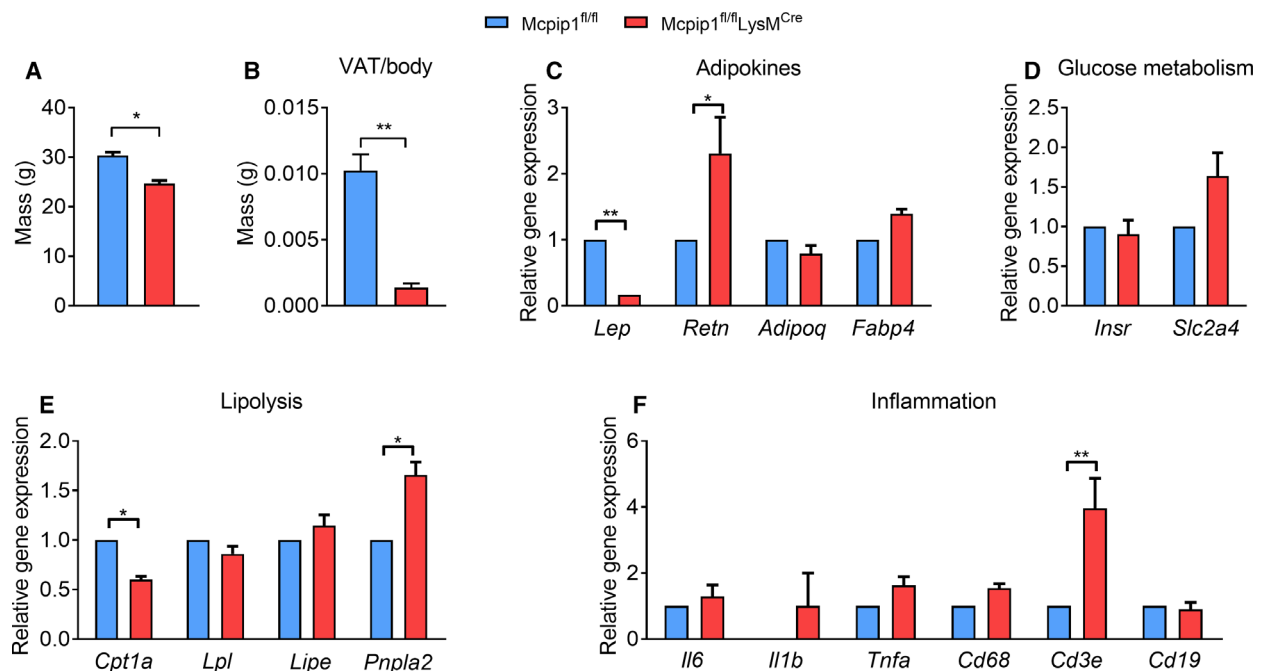


Fig. 6. Myeloid deletion of *Mcpip1* impairs functions of white adipose tissue. (A) Mass of 22-week-old *Mcpip1^{fl/fl}* and *Mcpip1^{fl/fl}LysM^{Cre}* mice and (B) visceral adipose tissue/body ratio; expression of genes in VAT from 22-week-old mice: (C) adipokines; (D) genes regulating glucose metabolism; (E) lipolysis; and (F) genes related to inflammation. Mean \pm SEM, for *Mcpip1^{fl/fl}*, $n = 6$ (A, B) and $n = 4$ (C–F); for *Mcpip1^{fl/fl}LysM^{Cre}*, $n = 3$ * $P < 0.05$, ** $P < 0.01$.

monocytes, and lymphocytes B markers (*Cd68*, *Cd19*) were not changed, but myeloid deletion of *Mcpip1* led to enhanced T lymphocyte infiltration into VAT (increase of *Cde3* level by 295%, Fig. 6F). Again, there were no differences between *Mcpip1*^{fl/fl}*Alb*^{Cre} and *Mcpip1*^{fl/fl} mice (data not shown). VAT of *Mcpip1*^{fl/fl}*LysM*^{Cre} mice fed with HFD was also characterized by low *Lep* and high *Retn* mRNA levels in comparison with controls (Fig. S8A). Additionally, myeloid deletion of *Mcpip1* led to a reduced amount of *Insr* mRNA and lipolysis-related genes (*Cpt1a*, *Lpl*, *Lipe*) with concomitant increase in *Il1b* and *Cd3e* transcripts (Fig. S8B–D).

At 10 weeks of age, indirect calorimetry analyzing energy expenditure showed no differences between *Mcpip1*^{fl/fl}*LysM*^{Cre} and control littermates (Fig. S9). Twenty-two-week-old *Mcpip1*^{fl/fl}*LysM*^{Cre} mice were characterized by diminished oxygen consumption, reduced carbon dioxide production resulting in significant drop of energy expenditure. Thus, increased energy burning cannot explain phenotype of mice with myeloid depletion of *Mcpip1*.

Myeloid *Mcpip1* deletion causes hypothermia and impairs locomotor activity

In the next set of experiments, we analyzed brown adipose tissue (BAT) collected from 10- and 22-week-old *Mcpip1*^{fl/fl} and *Mcpip1*^{fl/fl}*LysM*^{Cre} mice. At 10 weeks, there was no difference in BAT mass (0.003 ± 0.0003 vs 0.003 ± 0.0005 g), but its weight was significantly reduced in 22-week-old *Mcpip1*^{fl/fl}*LysM*^{Cre} knockouts (0.002 ± 0.0001 vs 0.003 ± 0.0002 g, Fig. 7A). Although the expression of thermoregulatory genes, namely uncoupling protein 1 (*Ucp1*) and peroxisome proliferator-activated receptor gamma coactivator 1-alpha (*Ppargc1a*), was not changed in young mice, there was a downregulation of both transcripts at 22 weeks by 95.7% and 54.2%, respectively (Fig. 7B). Similarly, myeloid deletion of *Mcpip1* led to enhanced monocytes and T lymphocytes infiltration into BAT (139% increase of *Cd68*, and 644% of *Cde3* levels) and increased *Tnfa* mRNA level by 624% in 22-week-old, but not in 10-week-old mice (Fig. 7C,D). Apart from diminished expressions of *Ucp1* and *Ppargc1a*, 22-week-old *Mcpip1*^{fl/fl}*LysM*^{Cre} knockouts were characterized by hypothermia (35.5 °C vs 37.6 °C in controls) (Fig. 7E). Finally, it is well known that reduced locomotor activity is a major contributor to diet-induced obesity in mice [27]. That is why, in the last set of experiments, we investigated both average velocity and total traveled distance by 10- and 22-week-old *Mcpip1*^{fl/fl}*LysM*^{Cre} and *Mcpip1*^{fl/fl}*Alb*^{Cre} knockouts.

Locomotor activity of all strains at 10 weeks was the same (Fig. 7F,G). However, 22-week-old *Mcpip1*^{fl/fl}*LysM*^{Cre} mice were characterized by significantly reduced locomotor activity. Although the average velocity of *Mcpip1*^{fl/fl}*LysM*^{Cre} was not changed, their total traveled distance was reduced by 70% in comparison with *Mcpip1*^{fl/fl} mice (Fig. 7F,G).

Discussion

We have previously demonstrated that hepatic steatosis accompanying diet-induced obesity diminishes the amount of *Mcpip1* protein in murine primary hepatocytes [28]. Similarly, the *Mcpip1* protein levels were reduced in murine and human adipose tissue collected from obese individuals [11,28]. Additionally, *Mcpip1* was shown to regulate lipid and glucose metabolism in hepatic and adipose tissue. Mechanistically, in hepatocytes *Mcpip1* induces both the expression and activity of hepatic peroxisome proliferator-activated receptor gamma via the TXNIP/PGC-1 α pathway [28]. On the other hand, in 3T3-L1 cells, the downregulation of *MCPIP1* at early stages of differentiation promotes the conversion of preadipocytes to adipocytes, resulting in an accumulation of fat. Conversely, an overexpression of *MCPIP1* in 3T3-L1 cells impaired adipogenesis by the direct cleavage of *C/EBP β* mRNA and selected pre-miRNAs [9,10]. However, the metabolic role of *Mcpip1* was not analyzed in tissue-specific knockout animals.

In the present study, we compared how deletion of *Mcpip1* in the myeloid leukocytes or in hepatocytes changes metabolism in response to chow or high-fat diet. We demonstrated a lack of metabolic manifestation in *Mcpip1*^{fl/fl}*Alb*^{Cre} mice fed chow or HFD food. Although *Mcpip1* knockout in hepatocytes reduces the expression of genes involved in glucose metabolism (*Pck1*, *G6pc*, *Irs1*) in liver, plasma glucose concentration was not changed when compared to *Mcpip1*^{fl/fl} counterparts. Similarly, the lack of *Mcpip1* in hepatocytes did not influence lipid metabolism in livers of mice fed chow or HFD. Notably, our observations are in accordance with another study, demonstrating that the deletion of *Mcpip1* in *Mcpip1*^{fl/fl}*Alb*^{Cre} mice is asymptomatic, in terms of blood morphology, cytokines, and chemokines detected in plasma. Instead, it leads to a massive hyperplasia of cholangiocytes and the development of primary biliary cholangitis [23]. The important role of *Mcpip1* in regulation of hepatic homeostasis was recently demonstrated by Sun and coworkers. By using mice with *Zc3h12a* deletion and overexpression in liver cells, the authors proved that *Mcpip1* functions to ameliorate liver damage, reduce

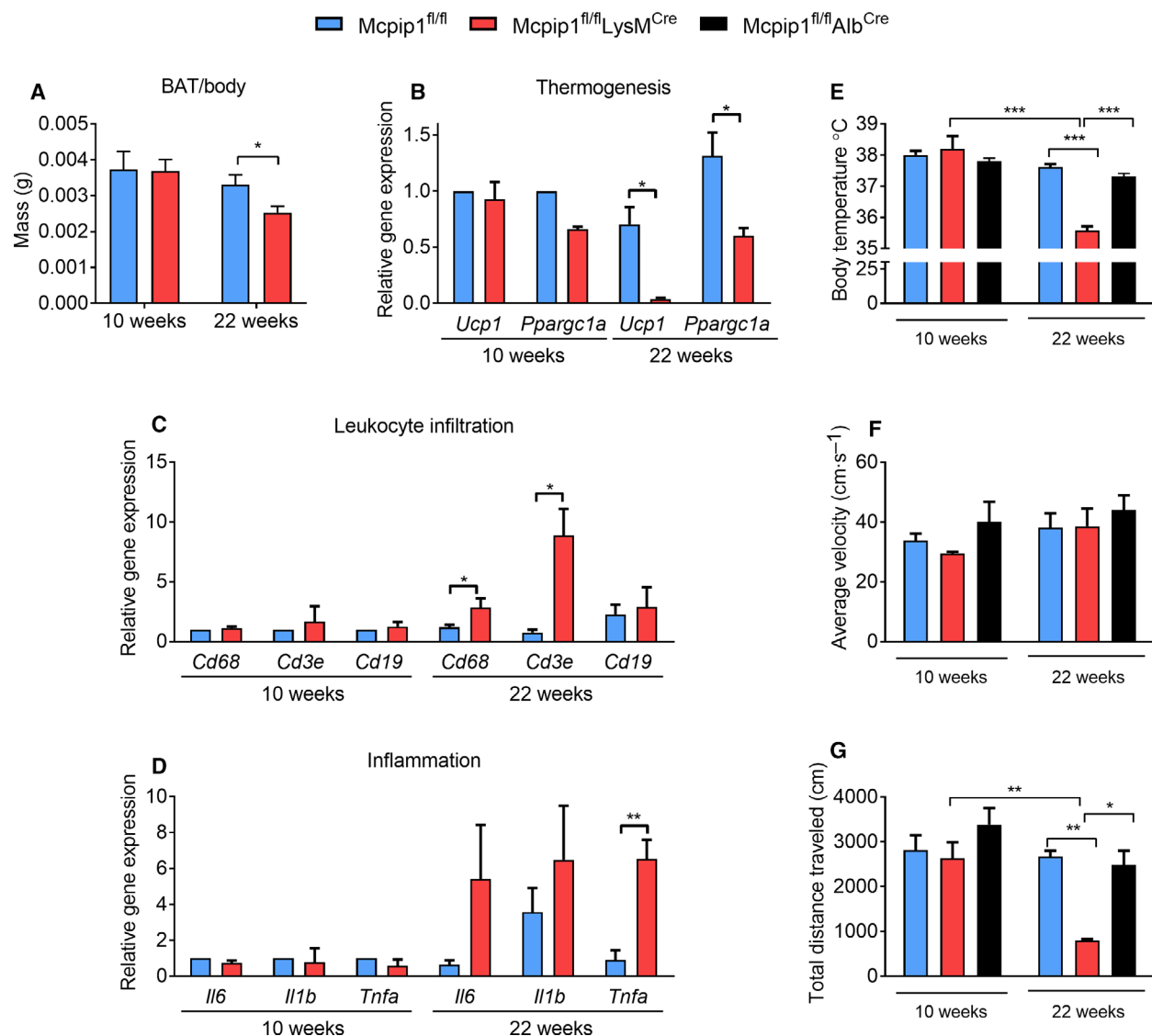


Fig. 7. Myeloid *Mcpip1* deletion impairs locomotor activity and causes hypothermia. (A) Mass of brown adipose tissue; expression of genes involved in (B) thermoregulation and (C) leukocyte infiltration; (D) inflammation; (E) body temperature; (F) average velocity and (G) total distance traveled. For *Mcpip1*^{fl/fl}, $n = 5$ (A–D) and $n = 10$ (E–G); for *Mcpip1*^{fl/fl}*LysM*^{Cre}, $n = 3$ (A–D) and $n = 5$ (E–G); and for *Mcpip1*^{fl/fl}*Alb*^{Cre}, $n = 6$. The graphs show means \pm SEM; * $P < 0.05$; ** $P < 0.01$; *** $P < 0.001$.

inflammation, prevent cell death, and promote regeneration after ischemia/reperfusion (I/R) injury [15]. The protective function of *Mcpip1* was mediated by increasing hypoxia-inducible factor 1 α expression [15]. Additionally, *Mcpip1* regulates the outcome of liver I/R through modifying macrophage polarization. *Mcpip1* knockdown shifted the balance of M1/M2 status toward M1 via the sensitization of the NF- κ B p65 pathway leading to deteriorated disease [29].

In contrast to *Mcpip1*^{fl/fl}*Alb*^{Cre} mice, the deletion of *Mcpip1* in myeloid leukocytes was strongly manifested. *Mcpip1*^{fl/fl}*LysM*^{Cre} animals at 22 weeks of age were

characterized by dyslipidemia, low plasma glucose level, disturbed liver homeostasis, and systemic proinflammatory phenotype, together with lethargy and hypothermia. Our observations are in line with the first characterization of *Mcpip1*^{fl/fl}*LysM*^{Cre} mice done by Li and coworkers, who described that after 5 months of age, mice failed to thrive and developed cachexia, splenomegaly, lymphadenopathy, and multi-organ inflammation [22]. Late-onset inflammatory syndrome described in *Mcpip1*^{fl/fl}*LysM*^{Cre} mice by Dobosz and coworkers was also observed in our diet-induced obesity model [30]. Twenty-two-week-old

myeloid-specific Mcpip1 knockout mice developed splenomegaly, significant systemic inflammation manifested by increased concentrations of proinflammatory cytokines and chemokines, compared with Mcpip1^{fl/fl} controls. In the livers of Mcpip1^{fl/fl}LysM^{Cre} mice, we also observed leukocyte infiltration, bile duct pathology, and extramedullary hematopoiesis (EMH). The pathologic EMH may be caused by one of many hematological diseases, bone marrow irradiation, or anemia [31,32]. It can be also seen as part of the response to infection or systemic inflammation [31,32], detected in fact in both total and myeloid-specific Mcpip1 knockouts [3,12,22]. Additionally, Kidoya and coworkers have shown that the post-transcriptional regulation mediated by Mcpip1 is essential for hematopoietic stem and progenitor cell homeostasis. Mcpip1 regulates self-renewal of hematopoietic stem and progenitor cells through modulating the stability of *Gata2* and *Tal1* mRNA, and its dysfunction leads to the rapid onset of abnormal hematopoiesis [33].

Similarly to our results, total Mcpip1 knockout mice displayed a decrease in serum levels of HDL-cholesterol and total triglycerides, but an increase in LDL/VLDL-cholesterol levels when compared to wild-type mice [34]. As demonstrated here, this phenotype cannot be attributed to Mcpip1 depletion in hepatocytes, since dyslipidemia was detected only in Mcpip1^{fl/fl}LysM^{Cre}, but not in Mcpip1^{fl/fl}Alb^{Cre} mice. According to Pin *et al.*, an increased level of LDL is dependent on HDL level reduction, due to the fact that LDL maturation requires the acquirement of cholesterol esters from HDL particles. If this process is disturbed, low-density, cholesterol-poor LDL particles lose their affinity to LDL receptors and remain in circulation [35]. High level of LDL-cholesterol in Mcpip1^{-/-} mice was also explained by the reduced expression of LDL-receptor in hepatocytes [34]. In addition, it was shown that high resistin level—observed also in VAT of myeloid Mcpip1 knockouts—induces degradation of LDL—receptor via PCSK9 protease [36].

In our opinion, changes in lipid and glucose metabolisms in Mcpip1^{fl/fl}LysM^{Cre} mice are secondary to the inflammatory syndrome, rather than a direct product of myeloid leukocytes Mcpip1 activity on the control of hepatic metabolism. In fact, low plasma glucose level and dyslipidemia are common features of murine sterile inflammation and cachexia models [35,37–40]. The low plasma glucose level in Mcpip1^{fl/fl}LysM^{Cre} mice might be explained by the altered expression of genes encoding proteins involved in gluconeogenesis (*G6pc*), insulin response (*Irs1*, *Irs2*), and glucose bidirectional transport (*Slc2a2*). Additionally, a raised level

of Tnf α in the plasma of these mice could account for decreased gluconeogenesis rates [41]. Twenty-two-week-old Mcpip1^{fl/fl}LysM^{Cre} mice were also characterized by a decreased mass of visceral adipose tissue and altered profile of adipokine expression. A lower mass of VAT in Mcpip1^{fl/fl}LysM^{Cre} animals correlated with reduced leptin expression that was earlier shown to be released from white adipose tissue in proportion to the size of fat depots [42]. Leptin, by inhibiting food intake, increases energy expenditure via the inhibition of lipogenesis and stimulation of lipolysis functions as a negative feedback signal in the regulation of energy balance. A low level of leptin may also explain the reduced expression of genes involved in beta-oxidation like *Ppara* or *Cpt1a* [42]. A reduced serum leptin level was also observed under nonobese physiological conditions in mice with depleted tissue macrophages. Macrophage depletion led to systemic inflammation induced by neutrophil infiltration and reduced body fat mass due to reduced energy intake [43].

Immune cell infiltration, such as macrophages and T cells, into white adipose tissue is an established phenomenon related to the pathophysiology of this tissue, especially in relation to obesity and diabetes [44]. Additionally, recent transcriptomic studies of BAT from HFD-induced obese mice demonstrated enhanced expression of gene markers for leukocytes, monocytes, and macrophages in these mice [45–47]. In BAT of 22-week-old Mcpip1^{fl/fl}LysM^{Cre} mice, we detected high levels of *Cd68* and *Cd3e* with concomitant reduction of genes regulating thermogenesis (*Ucp1*, *Ppargc1a*). It had already been shown that proinflammatory M1 macrophages infiltrating BAT impair its ability to appropriately respond to thermogenic stimuli, by the secretion of TNF α and IL-1 β that suppress the induction of *Ucp1* gene expression [48,49]. Since Mcpip1 inhibits the classic activation of M1 macrophages and promotes M2 polarization, we postulate that the hypothermia of Mcpip1^{fl/fl}LysM^{Cre} mice might be at least partially explained by an increased infiltration of M1 macrophages into BAT and a high level of *Tnfa* [29,50].

Finally, Mcpip1^{fl/fl}LysM^{Cre} mice did not develop hepatic steatosis, despite being fed a HFD. This kind of obesity-resistant phenotype was already described in methyl-CpG-binding domain 2 knockout mice (*Mbd2*^{-/-}) and in animals bearing a C305F mutation in the mouse double minute 2 homolog (*Mdm2*^{C307F}) [51,52]. *Mbd2* deficiency in mice fed HFD led to reduced epididymal adipose tissue mass, improved glucose tolerance, hyperlipidemia, and attenuated HFD-induced hepatosteatosis, features also present in Mcpip1^{fl/fl}LysM^{Cre} animals. However, our model

differs from *Mbd2*^{-/-} mice in respect to energy expenditure, adipose inflammation, and lipolysis [51]. Also, Liu and coworkers described that *Mdm2*^{C305F} mice demonstrated decreased fat accumulation along with improved glucose tolerance and increased energy expenditure after prolonged HFD feeding [52]. In contrast to the models mentioned above, myeloid deletion of Mcpip1 led to diminished oxygen consumption and reduced carbon dioxide production, resulting in a significant drop of energy expenditure. Thus, increased energy burning cannot explain the lean phenotype of Mcpip1^{fl/fl}LysM^{Cre} mice, but perhaps fecal energy loss could explain this phenomenon. Additionally, mice analyzed at 22 weeks of age did not have enhanced lipolysis nor reduced inflammation, such as *Mbd2*^{-/-} or *Mdm2*^{C307F} animals. A future study, utilizing 4-week-old animals fed with HFD, might help to understand this phenomenon, because young Mcpip1^{fl/fl}LysM^{Cre} animals do not have a proinflammatory phenotype that might influence obesity development. According to results published by Li and coworkers in 2-month-old myeloid Mcpip1 knockouts and Mcpip1^{fl/fl} controls, there were no differences in serum concentrations of proinflammatory cytokines and chemokines. Additionally, minimal inflammation in the lungs and livers of Mcpip1^{fl/fl}LysM^{Cre} mice was detected at 3 months of age, whereas inflammatory cell infiltration was significant at 6 months [22]. Diminished intestinal food assimilation might be an alternative explanation of resistance to high-fat diet-induced obesity in Mcpip1^{fl/fl}LysM^{Cre} mice. Although we do not have experimental data to support this view, this kind of molecular mechanism has already been described. Recently, the genetic inactivation of the Golgi-resident protein GRASP55 in mice was demonstrated to reduce whole-body fat mass via impaired intestinal fat absorption, causing resistance to high-fat diet-induced body weight gain [53].

In conclusion, we have demonstrated that the depletion of Mcpip1 in myeloid leukocytes results in systemic inflammation, dyslipidemia, low plasma glucose level, and disturbed liver lipid metabolism protecting from HFD-induced obesity. On the other hand, Mcpip1^{fl/fl}Alb^{Cre} mice did not exhibit signs of systemic inflammation, nor disturbed glucose and lipid metabolisms.

Materials and methods

Animals, diets, and genotyping

To obtain myeloid or hepatocyte-specific knockout of Mcpip1 protein, we used Mcpip1^{fl/fl} mice with two LoxP

sites flanking the two sides of exon 3 of the *Zc3h12a* gene encoding Mcpip1 [22]. Next, these mice were crossed with myeloid cells (LysM^{CreTg/Wt}, Jackson Laboratory; Bar Harbor, ME, USA; 004781) or hepatocytes expressing Cre transgenic mice (Alb^{CreTg/Wt}, Jackson Laboratory; Bar Harbor, Maine, United States of America; 018961). In the second round of crosses, Mcpip1^{fl/fl} females were crossed with Mcpip1^{fl/fl} LysM^{CreTg/Wt} males to obtain both control Mcpip1^{fl/fl} LysM^{CreWt/Wt} animals (designed as Mcpip1^{fl/fl}) and Mcpip1^{fl/fl} LysM^{CreTg/Wt} knockouts (designed as Mcpip1^{fl/fl}LysM^{Cre}). Similarly, Mcpip1^{fl/fl} females were crossed with Mcpip1^{fl/fl}Alb^{CreTg/Wt} males to obtain controls (Mcpip1^{fl/fl}) and knockouts (Mcpip1^{fl/fl}Alb^{Cre}). In all studies, C57BL/6N male mice were used that were fed *ad libitum* for 12 weeks with a chow diet (ZooLab; AIN93G) or HFD, (60% kcal from fat) (ZooLab; DP-1E-60S), starting from the age of 10 weeks. Animals were housed under SPF conditions in ventilated cages in a temperature-controlled environment with a 14/10-h light/dark cycle. To measure the amount of consumed food, the mice were housed in metabolic cages (Tecniplast; Buguggiate, Italy; 3600M021). For genotyping, DNA was extracted from tail tissue with a KAPA Mouse Genotyping Kit (KAPA Biosystems; Woburn, MA, USA; KK7302) according to the manufacturer's instructions. Sequences of primers (Sigma; Saint Louis, MO, USA) used for genotyping are listed in Table S1. All animal procedures were conducted in accordance with the Guide for the Care and Use of Laboratory Animals (Directive 2010/63/EU of the European Parliament) and carried out under a license from the 2nd Local Institutional Animal Care and Use Committee in Kraków (study no. 106/2017 and 360/2020).

Blood and tissue samples

Mice were fasted for 4 h, before their blood was collected from the orbital sinus after isoflurane anesthesia into EDTA (MP Biomedicals; Santa Ana, CA, USA; 195173) containing tubes, and then, the animals were euthanized. Plasma was prepared by centrifugation (1000 g, 10 min) and stored at -80 °C. Following euthanasia by cervical dislocation, organs were isolated and prepared for histological analysis, or snap-frozen in liquid nitrogen and stored at -80 °C.

Plasma analysis

Murine plasma was used for the subsequent analysis: cholesterol, HDL-cholesterol (HDL), LDL-cholesterol (LDL), glucose, triglycerides, alanine aminotransferase (ALT), aspartate aminotransferase (AST), and lactate dehydrogenase (LDH). These parameters were measured using an automatic biochemical analyzer, Pentra 400 (Horiba; Kyoto, Japan), by an enzymatic photometric method according to the vendor's instructions.

Glucose tolerance test

A glucose tolerance test (GTT) was performed on mice aged 22 weeks. Mice were fasted for 4 h, after which they were intraperitoneally injected with saturated glucose (Sigma; G7021) solution (2 g·kg⁻¹ body weight). Blood was collected from the tail vein before (0 min) and at 15, 30, 45, 60, 120 min after glucose application. Glucose concentrations were measured by an Accu-Check glucometer (Roche Diagnostics; Basel, Switzerland). The area under the curve (AUC) of blood glucose concentration was calculated geometrically by applying a trapezoidal method [54].

Histological analysis

Livers were fixed in 4% paraformaldehyde formalin solution (Chempur; Piekary Śląskie, Poland; 114321730) and divided into two parts. One piece was submerged in a 30% sucrose solution overnight for cryoprotection and then frozen in OCT medium (Tissue-Tek; Sakura, Tokyo, Japan; 4583) at -80 °C. Frozen sections were stained using an Oil Red O (ORO) method to analyze fat accumulation and imaged under 100× magnification. Ten images of each section were randomly collected and analyzed by the COLUMBUS v.2.4.2 software (Perkin Elmer; Waltham, Massachusetts, USA) with an algorithm adapted for Oil Red O-stained sections. The second piece was processed using standard paraffin procedures, and 5-μm paraffin tissue sections were stained with hematoxylin and eosin (H&E) for general histology and Picro Sirius Red (PSR) for collagen deposition and then visualized using a standard light microscope (Olympus BX51; Olympus Corporation, Tokyo, Japan).

Luminex assay

Magnetic Luminex Assay (R&D Systems; Minneapolis, MN, USA; LXSAMSM) was performed on plasma samples, according to the manufacturer's instructions. All samples were analyzed in duplicate on a MAGPIXs (Luminex, Austin, TX, USA). Median fluorescence intensity (MFI) data, obtained using a weighted 5-parameter logistic curve-fitting method, was used to calculate analyte concentrations.

RNA isolation and RT-PCR

Total RNA was isolated from liver tissue using a modified guanidinium isothiocyanate method [55]. Briefly, fragments of frozen liver tissue were lysed in fenzol (A&A Biotechnology; Gdansk, Poland; 203-50), and after addition of chloroform (POCH; Gliwice, Poland; 234431116), the aqueous phase containing RNA was collected into new Eppendorf tubes. Next, RNA was precipitated, centrifuged, washed in ethanol (POCH; Gliwice, Poland; 396420113), and finally dissolved in nuclease-free water (Sigma;

W4502). The concentration of RNA was assessed by a NanoDrop 1000 Spectrophotometer (Thermo Fisher Scientific; Waltham, MA, USA). Reverse transcription was performed using 1 μg of total RNA, oligo(dT) primer (Sigma) and M-MLV reverse transcriptase (Promega; Madison, WI, USA; M170B). Real-time PCR was carried out using Sybr Green Master Mix (A&A Biotechnology; 2008-100A) and QuantStudio Real-Time PCR System (Applied Biosystems; Waltham, MA, USA). Gene expression was normalized to elongation factor-2 (EF2), after which the relative level of transcripts was quantified by a 2^{-ΔΔCT} method. Sequences of primers (Genomed/Sigma) and annealing temperatures are listed in Table S2. The primers were designed to cross an exon-exon boundary to allow the specific amplification of cDNA targets.

Measurement of body temperature

Mice body temperature was measured by rectal probing (physiological monitoring unit THM150; Visualsonics, Toronto, Canada). The probe was inserted for 2 cm into the rectum and held in position for 10 s before temperature was determined. Measurements were conducted for five days at exactly the same time of day.

Open-field test

All mice were handled for three consecutive days prior to the start of behavioral measurements. On the day of the behavioral experiment, the mice were brought in their home cages to the testing room and left for 1 h to acclimate. General locomotor activity and movement velocity were monitored in an open field in arena cages (40 × 40 × 38 cm) made from transparent plexiglass, equipped with an array of infrared photo beams and software for automatic tracking of mouse ambulation (Activity Monitor 7, Med Associates Inc., St. Albans, VT, USA). The open-field arena was illuminated with white light at a level of 150 lux. The duration of each behavioral session was 30 min for each animal. After each trial, the cages were wiped with 70% ethanol and left to dry. To eliminate the effect of circadian rhythm on locomotor activity, all mice were subjected to the open-field test between 6 and 9 pm.

Indirect calorimetry measurements

Indirect calorimetry was performed to assess energy expenditure in wild-type (Mcpip^{fl/fl}) and Mcpip^{fl/fl} LysM^{Cre} mice at 10 and 22 weeks of age. Animals were placed into individual cages—Columbus Instruments Comprehensive Lab Animal Monitoring System chambers (Oxymax/CLAMS; Columbus Instruments, Columbus, OH, USA). VCO₂ and VO₂ were measured after 24-h acclimatization period and calculated based on the input and output rates of O₂ consumption and CO₂ production. The respiratory exchange

ratio ($RER = VCO_2/VO_2$) and heat production [$kcal \cdot min^{-1} = (3.815 \times 1.232 \times RER) \times (VO_2)$] were calculated using software provided by the manufacturer (Columbus Instruments, Columbus, OH, USA). Data were normalized to body weight.

Statistical analysis

Results are expressed as mean \pm SEM. The exact number of experiments or animals used is indicated in the figure legends. One-way ANOVA with Tukey's *post hoc* test was applied for comparison of multiple groups. To analyze the effects of two variable factors, a two-way ANOVA was used. The *P* values are marked with asterisks in the charts (**P* < 0.05; ***P* < 0.01; ****P* < 0.001).

Acknowledgements

This work was supported by research grants from National Science Centre, Poland, no. 2015/19/D/NZ5/00254 and 2017/27/B/NZ5/01440 to JeKo.

Conflict of interest

The authors declare no conflict of interest.

Author contributions

NP contributed to conceptualization, methodology, investigation, writing—original draft, and visualization; DZ contributed to investigation and writing—review and editing; JoKo contributed to resources and writing—review and editing; EK contributed to investigation and writing—review and editing; KW-L contributed to investigation; AJ contributed to investigation; MF contributed to resources; JJ contributed to conceptualization and writing—review and editing; JeKo contributed to conceptualization, methodology, writing—original draft, supervision, project administration, and funding acquisition.

Ethics approval

All animal experiments were approved by the 2nd Local Institutional Animal Care and Use Committee in Kraków (study no. 106/2017). All institutional and national guidelines for the care and use of laboratory animals were followed.

Peer Review

The peer review history for this article is available at <https://publons.com/publon/10.1111/febs.16040>.

Data accessibility

Data can be shared upon request. For this purpose, please contact Corresponding Author.

References

- Miekus K, Kotlinowski J, Lichawska-Cieslar A, Rys J & Jura J (2019) Activity of MCPIP1 RNase in tumor associated processes. *J Exp Clin Cancer Res* **38**, 421.
- Mizgalska D, Wegrzyn P, Murzyn K, Kasza A, Koj A, Jura J, Jarzab B & Jura J (2009) Interleukin-1-inducible MCPIP protein has structural and functional properties of RNase and participates in degradation of IL-1 β mRNA. *FEBS J* **276**, 7386–7399.
- Matsushita K, Takeuchi O, Standley DM, Kumagai Y, Kawagoe T, Miyake T, Satoh T, Kato H, Tsujimura T, Nakamura H *et al.* (2009) Zc3h12a is an RNase essential for controlling immune responses by regulating mRNA decay. *Nature* **458**, 1185–1190.
- Dobosz E, Wilamowski M, Lech M, Bugara B, Jura J, Potempa J & Koziel J (2016) MCPIP-1, alias regnase-1, controls epithelial inflammation by posttranscriptional regulation of IL-8 production. *J Innate Immun* **8**, 564–578.
- Li M, Cao W, Liu H, Zhang W, Liu X, Cai Z, Guo J, Wang X, Hui Z, Zhang H *et al.* (2012) MCPIP1 down-regulates IL-2 expression through an ARE- independent pathway. *PLoS One* **7**, e49841.
- Wang W, Huang X, Xin HB, Fu M, Xue A & Wu ZH (2015) TRAF family member-associated NF- κ B activator (TANK) inhibits genotoxic nuclear factor κ B activation by facilitating deubiquitinase USP10-dependent deubiquitination of TRAF6 ligase. *J Biol Chem* **290**, 13372–13385.
- Wang K, Niu J, Kim H & Kolattukudy PE (2011) Osteoclast precursor differentiation by MCPIP via oxidative stress, endoplasmic reticulum stress, and autophagy. *J Mol Cell Biol* **3**, 360–368.
- Roy A, Zhang M, Saad Y & Kolattukudy PE (2013) Antidicer RNase activity of monocyte chemotactic protein-induced protein-1 is critical for inducing angiogenesis. *Am J Physiol Cell Physiol* **305**, C1021–C1032.
- Lipert B, Wegrzyn P, Sell H, Eckel J, Winiarski M, Budzynski A, Matlok M, Kotlinowski J, Ramage L, Malecki M *et al.* (2014) Monocyte chemoattractant protein-induced protein 1 impairs adipogenesis in 3T3-L1 cells. *Biochim Biophys Acta* **1843**, 780–788.
- Losko M, Lichawska-Cieslar A, Kulecka P, Paziewska A, Rumieniczek I, Mikula M & Jura J (2018) Ectopic overexpression of MCPIP1 impairs adipogenesis by modulating microRNAs. *Biochim Biophys Acta Mol Cell Res* **1865**, 186–195.
- Losko M, Dolicka D, Pydyn N, Jankowska U, Kedracka-Krok S, Kulecka M, Paziewska A, Mikula

- M, Major P, Winiarski M *et al.* (2020) Integrative genomics reveal a role for MCP1P1 in adipogenesis and adipocyte metabolism. *Cell Mol Life Sci* **77**, 4899–4919.
- 12 Liang J, Saad Y, Lei T, Wang J, Qi D, Yang Q, Kolattukudy PE & Fu M (2010) MCP-induced protein 1 deubiquitinates TRAF proteins and negatively regulates JNK and NF-kappaB signaling. *J Exp Med* **207**, 2959–2973.
 - 13 Yu F, Du F, Wang Y, Huang S, Miao R, Major AS, Murphy EA, Fu M & Fan D (2013) Bone marrow deficiency of MCP1P1 results in severe multi-organ inflammation but diminishes atherogenesis in hyperlipidemic mice. *PLoS One* **8**, e80089.
 - 14 Li Z, Han S, Jia Y, Yang Y, Han F, Wu G, Li X, Zhang W, Jia W, He X *et al.* (2019) MCP1P1 regulates ROR α expression to protect against liver injury induced by lipopolysaccharide via modulation of miR-155. *J Cell Physiol* **234**, 16562–16572.
 - 15 Sun P, Lu YX, Cheng D, Zhang K, Zheng J, Liu Y, Wang X, Yuan YF & Tang YD (2018) Monocyte chemoattractant protein-induced protein 1 targets hypoxia-inducible factor 1 α to protect against hepatic ischemia/reperfusion injury. *Hepatology* **68**, 2359–2375.
 - 16 Kleiner DE, Brunt EM, Van Natta M, Behling C, Contos MJ, Cummings OW, Ferrell LD, Liu Y-C, Torbenson MS, Unalp-Arida A *et al.* (2005) Design and validation of a histological scoring system for nonalcoholic fatty liver disease. *Hepatology* **41**, 1313–1321.
 - 17 Farrell GC & Larter CZ (2006) Nonalcoholic fatty liver disease: from steatosis to cirrhosis. *Hepatology* **43**, 99–112.
 - 18 Streba LA, Vere CC, Rogoveanu I & Streba CT (2015) NAFLD, metabolic risk factors, and hepatocellular carcinoma: an open question. *World J Gastroenterol* **21**, 4103–4110.
 - 19 Vonghia L, Van Herck MA, Weyler J & Francque S (2019) Targeting myeloid-derived cells: New frontiers in the treatment of non-alcoholic and alcoholic liver disease. *Front Immunol* **10**, 563.
 - 20 Stienstra R, Saudale F, Duval C, Keshtkar S, Groener JE, van Rooijen N, Staels B, Kersten S & Muller M (2010) Kupffer cells promote hepatic steatosis via interleukin-1beta-dependent suppression of PPARalpha activity. *Hepatology* **51**, 511–522.
 - 21 Gadd VL, Skoien R, Powell EE, Fagan KJ, Winterford C, Horsfall L, Irvine K & Clouston AD (2014) The portal inflammatory infiltrate and ductular reaction in human nonalcoholic fatty liver disease. *Hepatology* **59**, 1393–1405.
 - 22 Li Y, Huang X, Huang S, He H, Lei T, Saaoud F, Yu XQ, Melnick A, Kumar A, Papasian CJ *et al.* (2017) Central role of myeloid MCP1P1 in protecting against LPS-induced inflammation and lung injury. *Signal Transduct Target Ther* **2**, 17066.
 - 23 Kotlinowski J, Hutsch T, Czyzyska-Cichon I, Wadowska M, Pydyn N, Jaształ A, Kij A, Dobosz E, Lech M, Miekus K *et al.* (2021) Deletion of Mcpip1 in Mcpip1^{fl/fl} Alb^{Cre} mice recapitulates the phenotype of human primary biliary cholangitis. *Biochim Biophys Acta Mol Basis Dis* **1867**, 166086.
 - 24 Nguyen P, Leray V, Diez M, Serisier S, Bloc'h JL, Siliart B & Dumon H (2008) Liver lipid metabolism. *J Anim Physiol Anim Nutr* **92**, 272–283.
 - 25 Petinelli P & Videla LA (2011) Up-regulation of PPAR-gamma mRNA expression in the liver of obese patients: an additional reinforcing lipogenic mechanism to SREBP-1c induction. *J Clin Endocrinol Metab* **96**, 1424–1430.
 - 26 Schroeder-Glockler JM, Rahman SM, Janssen RC, Qiao L, Shao J, Roper M, Fischer SJ, Lowe E, Orlicky DJ, McManaman JL *et al.* (2007) CCAAT/enhancer-binding protein beta deletion reduces adiposity, hepatic steatosis, and diabetes in Lepr(db/db) mice. *J Biol Chem* **282**, 13717–13729.
 - 27 Bjursell M, Gerdin AK, Lelliott CJ, Egecioglu E, Elmgren A, Tornell J, Oscarsson J & Bohlooly-Y M (2007) Acutely reduced locomotor activity is a major contributor to Western diet-induced obesity in mice. *Am J Physiol Endocrinol Metab* **294**, E251–E260.
 - 28 Pydyn N, Kadluczka J, Kus E, Pospiech E, Losko M, Fu M, Jura J & Kotlinowski J (2019) RNase MCP1P1 regulates hepatic peroxisome proliferator-activated receptor gamma via TXNIP/PGC-1alpha pathway. *Biochim Biophys Acta Mol Cell Biol Lipids* **10**, 1458–1471.
 - 29 Xiaoming A, Wenbo J, Jinyi W, Bin W, Chunyang H, Qi C & Lianbao K (2020) Macrophage regnase-1 deletion deteriorates liver ischemia/reperfusion injury through regulation of macrophage polarization. *Front Physiol* **11**, 582347.
 - 30 Dobosz E, Lorenz G, Ribeiro A, Würf V, Wadowska M, Kotlinowski J, Schmaderer C, Potempa J, Fu M, Koziel J *et al.* (2021) Murine myeloid cell MCP1P1 suppresses autoimmunity by regulating B-cell expansion and differentiation. *Dis Model Mech* **14**. <https://doi.org/10.1242/dmm.047589>
 - 31 Sohawon D, Lau KK, Lau T & Bowden DK (2012) Extra-medullary haematopoiesis: a pictorial review of its typical and atypical locations. *J Med Imaging Radiat* **56**, 538–544.
 - 32 Kim CH (2010) Homeostatic and pathogenic extramedullary hematopoiesis. *J Blood Med* **1**, 13–19.
 - 33 Kidoya H, Muramatsu F, Shimamura T, Jia W, Satoh T, Hayashi Y, Naito H, Kunisaki Y, Arai F, Seki M *et al.* (2019) Regnase-1-mediated post-transcriptional regulation is essential for hematopoietic stem and progenitor cell homeostasis. *Nat Commun* **10**, 1072.

- 34 Moody J, Yang C, Sedinkin J & Chang Y (2020) Systemic MCP1P1 deficiency in mice impairs lipid homeostasis. *Curr Res Pharmacol Drug Discov* **1**, 1–9.
- 35 Pin F, Barreto R, Couch ME, Bonetto A & O'Connell TM (2019) Cachexia induced by cancer and chemotherapy yield distinct perturbations to energy metabolism. *J Cachexia Sarcopenia Muscle* **10**, 140–154.
- 36 Melone M, Wilsie L, Palyha O, Strack A & Rashid S (2012) Discovery of a new role of human resistin in hepatocyte low-density lipoprotein receptor suppression mediated in part by proprotein convertase subtilisin/kexin type 9. *J Am Coll Cardiol* **59**, 1697–1705.
- 37 Wu Y, Wu T, Wu J, Zhao L, Li Q, Varghese Z, Moorhead JF, Powis SH, Chen Y & Ruan XZ (2013) Chronic inflammation exacerbates glucose metabolism disorders in C57BL/6J mice fed with high-fat diet. *J Endocrinol* **219**, 195–204.
- 38 Tsoupras A, Lordan R & Zabetakis I (2018) Inflammation, not cholesterol, is a cause of chronic disease. *Nutrients* **10**, 604.
- 39 Kealy J, Murray C, Griffin EW, Lopez-Rodriguez AB, Healy D, Tortorelli LS, Lowry JP, Watne LO & Cunningham C (2020) Acute inflammation alters brain energy metabolism in mice and humans: role in suppressed spontaneous activity, impaired cognition, and delirium. *J Neurosci* **40**, 5681–5696.
- 40 O'Connell TM, Ardeshirpour F, Asher SA, Winnike JH, Yin X, George J, Guttridge D, He W, Wysong A, Willis MS *et al.* (2008) Metabolomic analysis of cancer cachexia reveals distinct lipid and glucose alterations. *Metabolomics* **4**, 216–225.
- 41 Goto M, Yoshioka T, Battelino T, Ravindranath T & Zeller WP (2001) TNF α decreases gluconeogenesis in hepatocytes isolated from 10-day-old rats. *Pediatr Res* **49**, 552–557.
- 42 Harris RBS (2013) Direct and indirect effects of leptin on adipocyte metabolism. *Biochim Biophys Acta* **1842**, 414–423.
- 43 Lee B, Qiao L, Kinney B, Feng GS & Shao J (2014) Macrophage depletion disrupts immune balance and energy homeostasis. *PLoS One* **9**, e99575.
- 44 Surmi BK & Hasty AH (2008) Macrophage infiltration into adipose tissue. *Future Lipidol* **3**, 545–556.
- 45 McGregor RA, Kwon EY, Shin SK, Jung UJ, Kim E, Park JHY, Yu R, Yun JW & Choi MS (2013) Time-course microarrays reveal modulation of developmental, lipid metabolism and immune gene networks in intrascapular brown adipose tissue during the development of diet-induced obesity. *Int J Obes (Lond)* **37**, 1524–1531.
- 46 Bae J, Ricciardi C, Esposito D, Komarnytsky S, Hu P, Curry BJ, Brown PL, Gao Z, Biggerstaff JP, Chen J *et al.* (2014) Activation of pattern recognition receptors in brown adipocytes induces inflammation and suppresses uncoupling protein 1 expression and mitochondrial respiration. *Am J Physiol Cell Physiol* **306**, C918–C930.
- 47 Villarroya F, Cereijo R, Villarroya J, Gavaldà-Navarro A & Giralt M (2018) Toward an understanding of how immune cells control Brown and Beige adipobiology. *Cell Metab* **27**, 954–961.
- 48 Goto T, Naknukool S, Yoshitake R, Hanafusa Y, Tokiwa S, Li Y, Sakamoto T, Nitta T, Kim M, Takahashi N *et al.* (2016) Proinflammatory cytokine interleukin-1 β suppresses cold-induced thermogenesis in adipocytes. *Cytokine* **77**, 107–114.
- 49 Sakamoto T, Nitta T, Maruno K, Yeh YS, Kuwata H, Tomita K, Goto T, Takahashi N & Kawada T (2016) Macrophage infiltration into obese adipose tissues suppresses the induction of UCP1 level in mice. *Am J Physiol Endocrinol Metab* **310**, E676–E687.
- 50 Zhang WC, Qin F, Wang XJ, Liu ZF, Zhu L, Zeng A, Zhang MZ, Yu NZ & Long X (2019) Adipose-derived stromal cells attenuate adipose inflammation in obesity through adipocyte browning and polarization of M2 macrophages. *Mediators Inflamm* **2019**, 1731540.
- 51 Cheng J, Song J, He X, Zhang M, Hu S, Zhang S, Yu Q, Yang P, Xiong F, Wang DW *et al.* (2016) Loss of Mbd2 protects mice against high-fat diet-induced obesity and insulin resistance by regulating the homeostasis of energy storage and expenditure. *Diabetes* **65**, 3384–3395.
- 52 Liu S, Kim TH, Franklin DA & Zhang Y (2017) Protection against high-fat-diet-induced obesity in MDM2^{C305F} mice due to reduced p53 activity and enhanced energy expenditure. *Cell Rep* **18**, 1005–1018.
- 53 Kim J, Kim H, Noh SH, Jang DG, Park SY, Min D, Kim H, Kweon HS, Kim H, Aum S *et al.* (2020) Grasp55^{-/-} mice display impaired fat absorption and resistance to high-fat diet-induced obesity. *Nat Commun* **11**, 1418.
- 54 Le Floch JP, Escuyer P, Baudin E, Baudon D & Perlemuter L (1990) Blood glucose area under the curve. Methodological aspects. *Diabetes Care* **13**, 172–175.
- 55 Chomczynski P & Sacchi N (1987) Single-step method of RNA isolation by acid guanidinium thiocyanate-phenol-chloroform extraction. *Anal Biochem* **162**, 156–159.

Supporting information

Additional supporting information may be found online in the Supporting Information section at the end of the article.

Fig. S1. Comparison of Mcpip1^{fl/fl} controls from Mcpip1^{fl/fl}LysM^{Cre} and Mcpip1^{fl/fl}Alb^{Cre} strains.

Fig. S2. Expression of *Zc3h12a* encoding Mcpip1 in the liver and white adipose tissue.

Fig. S3. Daily food intake, ALT and AST activity and liver mass of Mcpip1^{fl/fl}, Mcpip1^{fl/fl}LysM^{Cre} and Mcpip1^{fl/fl}Alb^{Cre} mice fed chow diet.

Fig. S4. Representative histology images of liver from mice fed chow diet.

Fig. S5. Daily food intake, ALT and AST activity and liver mass of Mcpip1^{fl/fl}, Mcpip1^{fl/fl}LysM^{Cre} and Mcpip1^{fl/fl}Alb^{Cre} mice fed HFD.

Fig. S6. Representative histology images of liver from mice fed HFD.

Fig. S7. Comparison of 10-week-old Mcpip1^{fl/fl} and Mcpip1^{fl/fl}LysM^{Cre} mice.

Fig. S8. Analysis of gene expression profile in visceral adipose tissue from HFD-fed Mcpip1^{fl/fl} and Mcpip1^{fl/fl}LysM^{Cre} mice.

Fig. S9. Indirect calorimetry measurements in Mcpip1^{fl/fl} and Mcpip1^{fl/fl}LysM^{Cre} mice.

Table S1. Sequences of primers used for genotyping.

Table S2. Sequences of primers used for real-time PCR.

Table S3. Immune profile of plasma samples from 22-week-old mice fed with HFD for 12 weeks, determined by Luminex Assay.